Journal of Applied Polymer Science

Electrical Energy Discharging Performance of Poly(vinylidene fluoride-*co*-trifluoroethylene) by Tuning Its Ferroelectric Relaxation with Polymethyl Methacrylate

Weimin Xia,[1,2] Qiuping Zhang,[2] Xiao Wang,[2] Zhicheng Zhang[2]

[1]Institute of Printing and Packaging Engineering, Xi'an University of Technology, Xi'an 710048, People's Republic of China
[2]Department of Applied Chemistry, School of Science, MOE Key Laboratory for Nonequilibrium Synthesis and Modulation of Condensed Matter, Xi'an Jiaotong University, Xi'an 710049, People's Republic of China
Correspondence to: W. Xia (E-mail: xia.weimin@stu.xjtu.edu.cn) and Z. Zhang (E-mail: zhichengzhang@mail.xjtu.edu.cn)

ABSTRACT: Poly(methyl methacrylate) (PMMA) was introduced into ferroelectric Poly(vinylidene fluoride-*co*-trifluoroethylene) P(VDF-*co*-TrFE) via a simple solution blending process and a series of P(VDF-*co*-TrFE)/PMMA blends with varied PMMA content was obtained in an effort to investigate the confinement effect of PMMA on the crystalline, dielectric, and electric energy storage properties of P(VDF-*co*-TrFE). PMMA addition could reduce the crystallinity dramatically as well as the crystal size due to its dilution effect and impediment effect on the crystallization of P(VDF-*co*-TrFE). PMMA introduction is also responsible for the phase transition of P(VDF-*co*-TrFE) from α phase into γ phase. As expected, both the dielectric constant and loss of the blends are reduced as PMMA addition increases for the dilute, decoupling, and confinement effect of PMMA on the relaxation behavior of crystal phases of P(VDF-*co*-TrFE) under external electric field. As a result, both the maximum and remnant polarization of the blends are significantly depressed. The irreversible polarization of P(VDF-*co*-TrFE) is effectively restricted by the addition of PMMA due to its impeding effect on the crystallization of P(VDF-*co*-TrFE) and restricting effect on the switch of the polar crystal domains. Therefore, the energy loss induced by the ferroelectric relaxation of P(VDF-*co*-TrFE) is significantly reduced to less than 25% at an electric field of 450 MV/m while the energy storage density is well maintained at about 10 J/cm^{-3} in the blend with 30 wt % PMMA. The results may help to understand how the ferroelectric relaxation affects the energy loss of ferroelectrics fundamentally and design more desirable materials for high energy storage capacitors. © 2013 Wiley Periodicals, Inc. J. Appl. Polym. Sci. **2014**, *131*, 40114.

KEYWORDS: dielectric properties; phase behavior; structure-property relations

Received 21 May 2013; accepted 26 October 2013
DOI: 10.1002/app.40114

INTRODUCTION

Poly(vinylidene fluoride) (PVDF)-based semicrystalline fluoropolymers have attracted a great deal of interests both in material science academy and microelectronics industry for their high dielectric constant (ca. 10–12 at 1 kHz for PVDF),[1–3] which could have a potential applications as the capacitor[4–6] and some other energy storage units because of their strong C-F and C-H dipoles. Unfortunately, limited success has achieved in improving the efficiency of energy density of PVDF-based fluoropolymers because of the relatively high remnant polarization in β-PVDF and VDF/TrFE copolymers at the high electrical strength.[7,8] Because the ferroelectric nature of the polymers makes their displacement-electric field hysteresis loops (D–E) in near rectangle shape. That means most of the stored energy is unable to be released once the applied electric field is removed or the capacitor is shot down. To overcome these hurdles, modification of PVDF-based fluoropolymers physically or chemically has been developed and reported during the past decades. In the physical route, electron irradiation was firstly reported to modify P(VDF-*co*-TrFE) in 1998.[9] *Via* tailoring the high polar crystal domains in long sequence into small pieces with high-energy electron beams, the Curie temperature of irradiated P(VDF-*co*-TrFE) is shifted to room temperature and D–E hysteresis loops are turned from normal ferroelectric profile in rectangle shape into a relaxed ferroelectric characterized with a slim loop. In the chemical route, certain amounts of bulky comonomers such as chlorotrifluoroethylene (CTFE) or hexafluoropropylene (HFP) were randomly incorporated into P(VDF-*co*-TrFE) main chains, which was aimed to reduce crystal size.[10,11] Since then, the copolymers or terpolymers have been extensively studied in academy and a great enhancement in energy density has been achieved.[12–19] For instance, special

treatments of P(VDF-*co*-CTFE), like stretching[15–17] or cured with UV light,[18] could even enhance the energy density up to 25 and 22.5 J/cm^{-3} under 600 MV/m field and 400 MV/m field, respectively. However, in spite of these exciting improvement in the energy density capability, PVDF based fluoropolymers still suffer from high energy loss (ca. 40–60% of overall energy charged), which limits their application in much wider fields.

It has been well studied that the high energy loss of PVDF-based polymers mainly comes from the internal friction between polar crystals domains result from polar molecular chains as their dipoles flip following an external electric field. The strong coupling interaction between adjacent high polar crystal domains is also found to be responsible for the high energy loss.[20] Besides, for the semicrystalline polymers, the polarization relaxation of the amorphous phase is rather long and thus results in a low releasing efficiency of energy stored at high frequency. Therefore, the fundamental idea to reduce the energy loss of PVDF-based polymers should be focused on accelerating the switching speed of the polar crystal domains either by reducing the crystallite size to lessen the coupling interaction between adjacent polar crystal domains or reducing the relaxation period of the amorphous phases during polarization. Recently, polystyrene (PS) grafted on P(VDF-*co*-CTFE) as side chains was proposed by Zhu L group.[21,22] As expected, the introduction of PS did reduce the dielectric and energy loss dramatically (below 20% at 500 MV/m). However, due to the poor compatibility between PS and P(VDF-*co*-CTFE) main chain, their weak intermolecular force limits the confining effect provided by PS in amorphous phase greatly.

According to previous research, amorphous PMMA with higher polarity has good compatibility with PVDF main chain and could effectively reduce the crystalline and dielectric properties of PVDF or P(VDF-*co*-TrFE) when blending into PVDF or P(VDF-*co*-TrFE).[23–30] Our previous study has already shown that the addition of rigid PMMA into PVDF amorphous phase could improve the modulus of PVDF and block its crystal phase transition from α- to γ-phase driven by the high electric field applied.[31] However, the phase transition dependence of electric properties of ferroelectric P(VDF-*co*-TrFE) has not been concerned. On the basis of this fact, we propose to blend PMMA with low TrFE mole content (9%) P(VDF-*co*-TrFE) possessing the multiple crystal phases in this work to illustrate how to tune the crystal phase transition and ferroelectric relaxation of P(VDF-*co*-TrFE) with PMMA added into the amorphous phase via reducing the crystal size of P(VDF-*co*-TrFE) crystal domains as well as restricting the switch of high polar crystal domains. With rigid PMMA filling in the amorphous area instead of P(VDF-*co*-TrFE) in rubber state, free space provided for the flipping of high polar domains is expected to be reduced and the relaxation response speed of the amorphous phase is expected to be improved. Meanwhile, we would like to provide direct evidence and fundamental investigation to show how the ferroelectric relaxation and the induced energy loss of P(VDF-*co*-TrFE) is controlled, which has never been mentioned in the previous study. Both the deep understanding and tuning of ferroelectric relaxation are important to design and modify PVDF based ferroelectric polymers in order to reduce the energy loss for energy storage applications.

EXPERIMENTAL

Materials

Raw material P(VDF-*co*-CTFE) (31508) containing 9 mol % CTFE was purchased from Solvay Solex. PMMA powder with a molecular weight of 410,000 was purchased from Alfa Aesar China (Tianjin). Matrix P(VDF-*co*-TrFE)s with 9 mol % TrFE molar ratio were synthesized by a full hydrogenation process of P(VDF-*co*-CTFE) following the procedure described in Ref. 32. The structure and the composition of P(VDF-*co*-TrFE) were confirmed by ^{1}H and ^{19}F-NMR. All the other chemicals were obtained from commercials and used as received.

Fabrication of P(VDF-*co*-TrFE)/PMMA Blend Films

The films about 10–20 μm in thick were fabricated via casting the uniform polymer blend solution as described below. First, a polymeric blend solution containing about 3 wt % polymer was prepared via dissolving the polymers in dimethylformamide (DMF) at 60°C for 12 h under vigorous stirring. Polymer films were obtained via casting the blend solution onto glass slides coated with PTFE (Polytetrafluoroetylene) at 70°C. After the solvent was evaporated completely, the glass slides were transferred into an oven and heated at 200°C for 12 h followed by immediately quenching into liquid nitrogen (−195.8°C). The samples were labeled as 0, 5%, 10%, 15%, 20%, 30%, and 40%, respectively to distinguish from each other by the weight percentage of PMMA contained.

Characterization

X-ray diffraction (XRD) results were obtained on a RIGAKU D/MAX-2400 (Rigaku Industrial, Japan). The wavelength of the X-ray was 1.542 Å (Cu Kα radiation, 40 kV and 100 mA) and the scanning velocity was 4°/min. Differential scanning calorimetry analysis (DSC) was conducted on a NETZSCH DSC 200 PC (NETZSCH, Germany) in nitrogen atmosphere at a heating rate of 5°C/min for the first circle. For electric characterizations, gold electrodes (thickness about 80 nm) were sputtered on both surfaces of the polymer films with a JEOL JFC-1600 Auto fine coater (Japan). The dielectric properties were measured at different frequencies and at 1 V on a Novocontrol Concept40 loop inductance, capacitance, and resistance (LCR) meter. The electric D–E hysteresis loops were measured on a Premiere II ferroelectric tester from Radiant Technologies, with a triangular wave form at 10 Hz. This measurement system has a preloop process on the sample to test the stability of the sample before outputting data. The electric fields were applied across the polymer films with an increment of 25 MV/m until the films were electrically broken down or to the limit of the machine (10,000 V).

RESULTS AND DISCUSSION

The Effect of PMMA Addition on the Crystalline Properties of P(VDF-*co*-TrFE)

The crystalline properties of P(VDF-*co*-TrFE) and PMMA blend films are characterized with DSC combined with XRD techniques as described in Ref. 33.

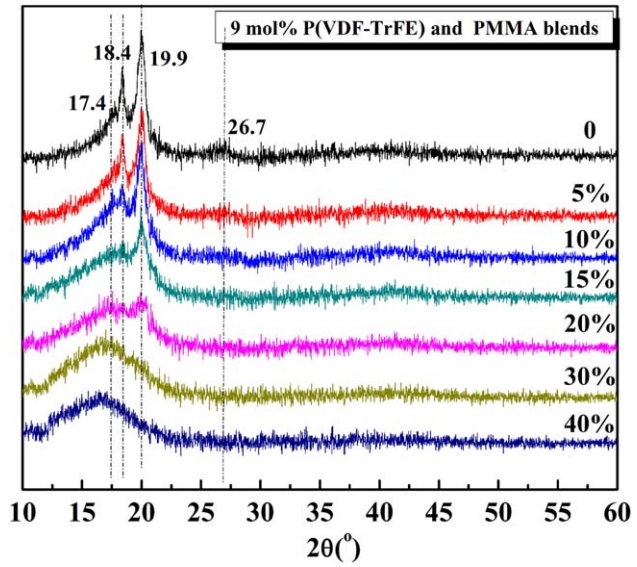

Figure 1. XRD spectra of P(VDF-*co*-TrFE) with 9 mol % TrFE and its blends containing varied PMMA content, with the numbers standing for the characteristic reflection peaks. [Color figure can be viewed in the online issue, which is available at wileyonlinelibrary.com.]

The influence of PMMA addition on the crystalline properties of P(VDF-*co*-TrFE) XRD was presented in Figure 1. Similar to neat PVDF, the α-phase of P(VDF-*co*-TrFE) is characterized with four discernable peaks at 17.4°, 18.4°, 19.9°, and 26.7°, corresponding to the Bragg diffractions of (100), (020), (110), and (021) of α-phase PVDF, respectively.[34–37] The *β*-phase could be identified by the single and sharp peak located at 19.7°, representing the Bragg diffraction of (110)/(200) plane.[35] As for *γ*-phase, the reflection is only observed at 18.4 and 19.9° and the intensity of the peak at 18.4° is much lower than that of 19.9°. However, if the crystalline region of the polymer possesses more than one type of crystalline phase, the reflection peaks of α-phase would overlap with those from *β*- and *γ*-phase, making it rather difficult to distinguish from each other. As shown in Figure 1, the characteristic reflection peaks of α-phase appeared at 17.4°, 18.4°, 19.9°, and 26.7° are sufficient clear to identify the presence of main α-phase when the PMMA content is less than 15 wt %. When the PMMA content is higher than 15 wt %, the intensities of these peaks are reduced greatly, indicating the decrease of the amount of α-phase. Moreover, the peaks are continuously widening as the PMMA content increases, which has been accounted for either the decrease of the ordering degree of the crystalline cells or the reduction of the crystal size.[25] As for the existence and the content of *β*- and *γ*-phase, they could hardly be identified from XRD of all the samples since the characteristic peaks of three kinds of crystal phases are all very close to 20° and overlapped together.

DSC thermograms have been recently proved to be a powerful method to identify and distinguish different crystal P(VDF-*co*-TrFE) phases from each other. Figure 2(a) shows the DSC curves of the quenched polymer blends with altered compositions for the first heating circle.[36–40] Apparently, multiple endothermic peaks are observed in all the samples indicating the coexistence of multiple types of crystalline phases in these samples as confirmed by FTIR and XRD results. It is reported that the melting points of α-, *β*-, and

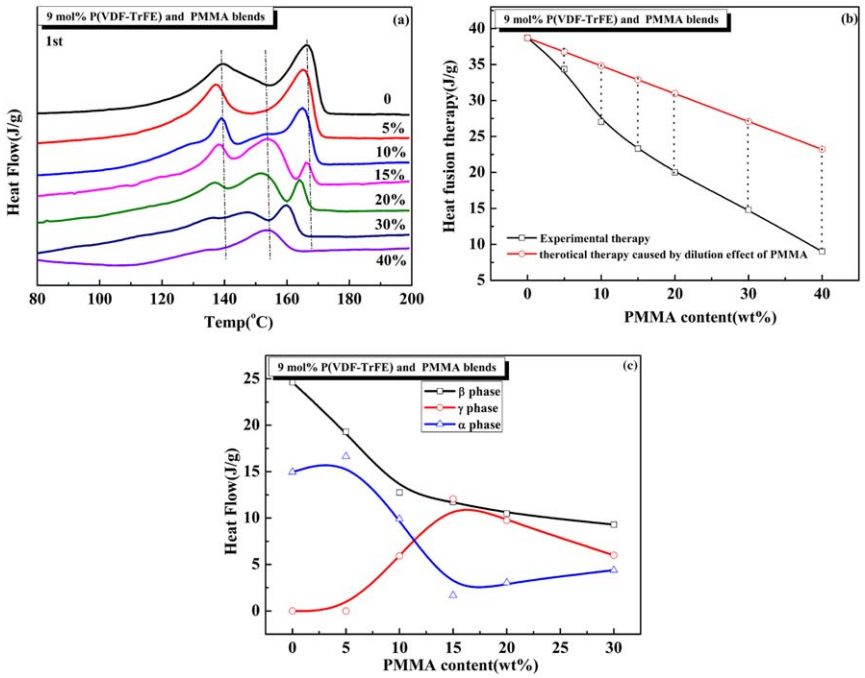

Figure 2. (a) DSC thermograms of P(VDF-*co*-TrFE) with 9 mol % TrFE and its blends containing varied PMMA content, with the dash dot lines to illustrate the change tendency of the melting point. (b) Overall ΔH_f of P(VDF-*co*-TrFE)/PMMA blends. The line with open rectangle symbol was the experimental results calculated from the integral of DSC thermograms. The line with open circle symbols was ΔH_f calculated by multiplying the ΔH_f of neat P(VDF-*co*-TrFE)with its weight percentage in the blends, where only dilution effect of PMMA was accounted. (c) ΔH_f of each crystal phase in P(VDF-*co*-TrFE)/PMMA blends. [Color figure can be viewed in the online issue, which is available at wileyonlinelibrary.com.]

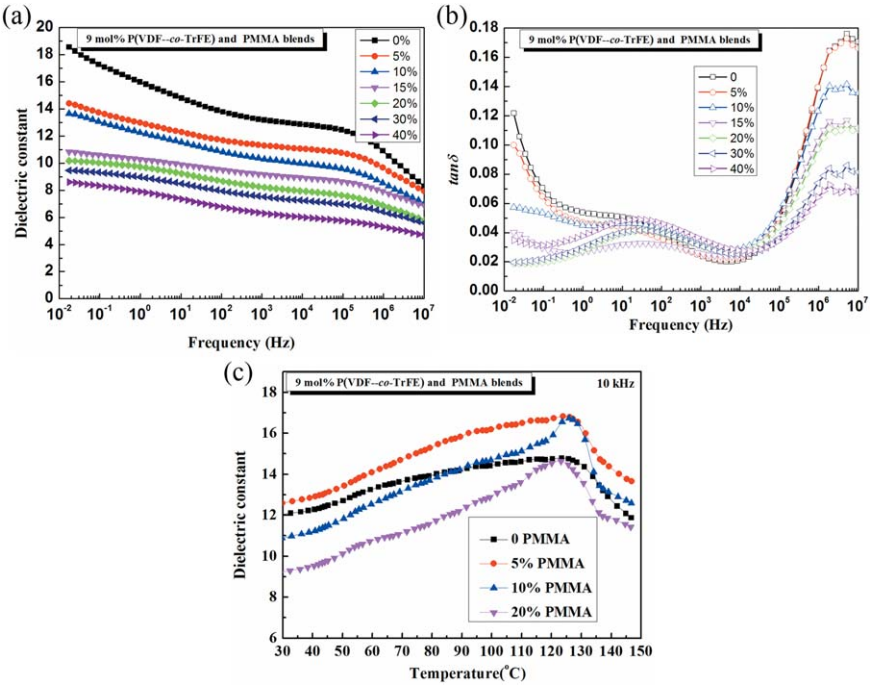

Figure 3. (a) Dielectric constant of P(VDF-*co*-TrFE)/PMMA blends as a function of frequency at room temperature. (b) Dielectric loss of P(VDF-*co*-TrFE)/PMMA blends as a function of frequency at room temperature. (c) Dielectric constant of P(VDF-*co*-TrFE)/PMMA blends as a function of temperature at 10 kHz. [Color figure can be viewed in the online issue, which is available at wileyonlinelibrary.com.]

γ-phases of P(VDF-*co*-TrFE) are about 170, 140, and 160°C, respectively depending on the content of TrFE in these crystals.[41] As shown in Figure 2(a), the crystalline region of neat P(VDF-*co*-TrFE) and the polymer blend with 5 wt % PMMA is mostly in β- and α-phase, while the samples containing 10–30 wt % PMMA possess β-, γ-, and α-phases. As for the blend with 40 wt % PMMA, only γ-phase is remained. It is known that PMMA with glass state delays the diffusion of molecules in the melting process of P(VDF-*co*-TrFE) and thus increased the probability of the stabilization of conformational fluctuations that resulted in the γ-phase formation.[42] The phase transition from α-phase was indicative of a melting and recrystallization process when the blends were heated to 200°C and quenched by liquid nitrogen. In addition, the melting point of each phase is slightly depressed as PMMA content increases from 0 to 40 wt %, clearly indicating the compatibility between PMMA and P(VDF-*co*-TrFE) above its melting point.[23]

The crystallinity of the blends could be calculated by the formula of $\chi_c = \Delta H_f / \Delta H_f^* \times 100\%$, where ΔH_f^* is the heat fusion enthalpy of P(VDF-*co*-TrFE) with 100% crystallinity. As χ_c is in liner relationship with ΔH_f and ΔH_f^* of P(VDF-*co*-TrFE) is not available, ΔH_f is directly utilized to follow the crystallinity change without further accurate calculation of χ_c. The ΔH_f of the blends is shown in Figure 2(b) as a function of PMMA content, where the line with open circle symbol represents the ΔH_f change caused only by the dilution effect of PMMA addition theoretically. The one with open rectangle symbol stands for that of ΔH_f obtained from DSC experimentally. Apparently, the experimental heat fusion enthalpy of the blends is much lower than that of theoretical results considering only the dilution effect of PMMA. That means PMMA introduced is impeding the crystallization of P(VDF-*co*-TrFE) more than just diluting P(VDF-*co*-TrFE) matrix. The ΔH_f of each crystal phase is separately obtained from the integrals of DSC curves and presented as a function of PMMA content in Figure 2(c). Clearly, the percentage of β-phase declines continuously as the PMMA content increases for the dilution effect. When PMMA content is less than 15 wt %, γ- and α-phase exhibits a complementary relationship, namely the percentage of γ-phase is enhanced while the content of α-phase is reduced simultaneously as PMMA increases, suggesting the conversion of crystal phase from α- to γ-phase. The previous study has shown that the introduction of PMMA in PVDF is one of the effective ways to achieve the crystal phase transition from antipolar α-phase to polar β- or γ-phase.[43] Considering the energy barriers for the α to γ transformation is less than that for α to β and γ to β transformation,[44] the crystal phase transition of P(VDF-*co*-TrFE) induced by PMMA addition is more preferable from α- to γ-phase based on the FTIR, XRD, and DSC results. When the content of PMMA is over 15 wt %, both α- and γ-phases are reduced due to the dilution effect.

In general, the addition of PMMA is affecting the crystalline properties of P(VDF-*co*-TrFE) including reducing the overall crystallization by impeding its nucleation as well as inducing the phase transition in P(VDF-*co*-TrFE).

Dielectric Constant and Loss of P(VDF-*co*-TrFE)/PMMA Blends

The effect of PMMA addition on the dielectric behavior of P(VDF-*co*-TrFE) at low electric fields (bias voltage = 1 V) is investigated by measuring the dielectric permittivity and loss as a function of broad frequency and the results are presented in Figure 3(a,b). The dielectric response of semicrystalline PVDF-

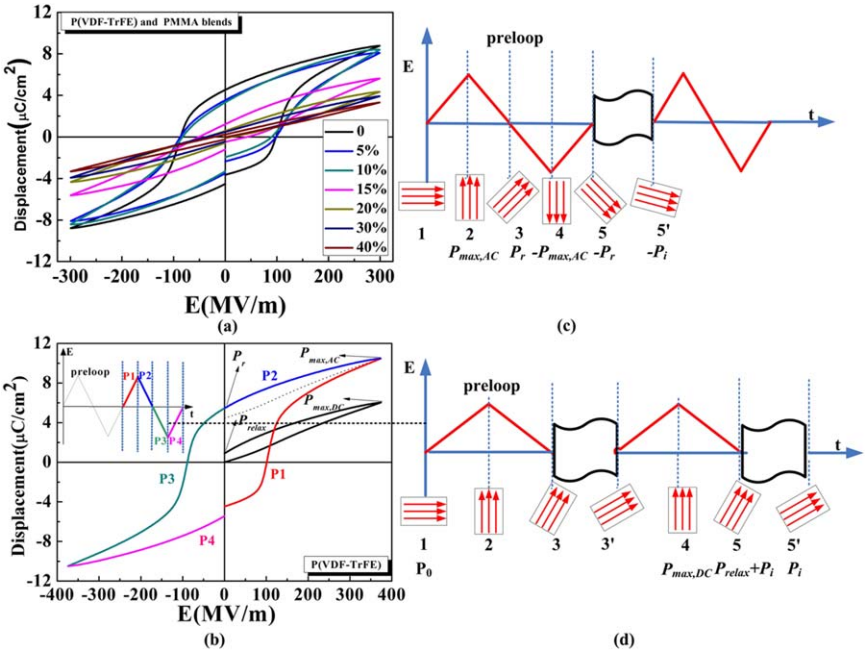

Figure 4. (a)The comparisons between the bipolar D–E loops of P(VDF-*co*-TrFE) with 9 mol % TrFE and its blends containing varied PMMA content at 300 MV/m. (b) The typical D–E hysteresis loops of ferroelectric P(VDF-*co*-TrFE) under high AC and DC electric field; (c) Illustration scheme of polarization process under AC and DC field (d). [Color figure can be viewed in the online issue, which is available at wileyonlinelibrary.com.]

based fluoropolymers under low electric field at frequency below 100 kHz has been well recognized to originate from both the dipoles alignment in amorphous phase in rubber state and the weak swing of crystal phase.[45] As frequency increases from 0.01 Hz to 1 MHz, the contribution of crystal phase is vanishing for the delay of the swing of crystal phase than the applied electric field characterized with a sharp increment of the dielectric loss at this frequency range. When the frequency is over 1 MHz, the dielectric response only comes from the two random molecular motions including the micro-Brownian motion of noncrystalline chain segments (β-relaxation)[45] and the molecular motion onto the amorphous/crystalline interfaces.[46–48] As indicated in Figure 3(a), PMMA addition leads to the continuous decrease of the dielectric permittivity between 0.01 Hz and 10 MHz depending on the PMMA content for the dilution effect of PMMA with much lower dielectric permittivity than P(VDF-*co*-TrFE). In addition, the strong intermolecular force between rigid PMMA segments and soft VDF units in amorphous phase may also result into the restricted dielectric response of high polar VDF units to the applied electric field. Moreover, Figure 3(b) shows the dielectric loss(tan δ) spectrum of different blends, and tan δ of PMMA insufficient blends decreases as the frequency increases at the range of 0.01–10 kHz, which could be attributed to the α-relaxation of crystalline phase of P(VDF-*co*-TrFE). After the frequency increased to 100 kHz, because of the influence of the amorphous phase relaxation (so called β-relaxation) as described in Ref. 45, the dielectric loss presents a reverse trend as it is at low frequency in the blends despite of PMMA contents. Besides, the addition of PMMA shows some influence on tan δ of P (VDF-*co*-TrFE)/PMMA blends at low frequency. It is reported that the peak of dielectric relaxation in glass forming PMMA below glass transition point ($T_g \sim 100$°C) is located at the range about 10–100 Hz.[49] Therefore, as presented in Figure 3(b), the appeared symmetrical relaxation peaks at the frequency around 20 Hz could result in the increasing tan δ in PMMA abundant (20–40 wt %) blends. However, as the frequency increase, the introduction of PMMA will significantly reduce tan δ at high frequency (ca. 5 kHz) as shown in Figure 3(b). Near 60% of tan δ is reduced from 0.17 of the neat P(VDF-*co*-TrFE) to 0.065 of the blend with 40 wt% PMMA at 10 MHz. That means the introduction of PMMA shows significant confinement on the relaxation of P(VDF-*co*-TrFE) content.

In addition, the temperature dependence of dielectric constant of different PMMA contents P(VDF-*co*-TrFE)/PMMA blends at 10 kHz were presented in Figure 3(c). Because of dielectric relaxation, the dielectric permittivity of all blends increases as the temperature below 125°C and shows the dielectric peak at about 120 to 130°C. The dielectric peaks do relate to the Curie temperature (T_c) of the P(VDF-*co*-TrFE) blends, which is recognized as the ferroelectric to paraelectric (F–P) transition point of polar β- or γ-phase. When the mole contents of PMMA are 0 and 5%, the dielectric peaks intensity of the blend is low. However, as the PMMA contents increased to 10% and 20%, the peaks intensity of the blends grows accordingly. The reason is that more antipolar α-phase is transformed to polar β- or γ-phase in PMMA abundant blends, which is consistent with DSC and XRD results.

D–E Hysteresis Loops of P(VDF-*co*-TrFE)/PMMA Blends

D–E hysteresis loops measurements are performed to investigate the dielectric properties of the blend films under high electric fields. Figure 4(a) compares the bipolar D–E loops of the blend films with varied PMMA content under the same AC electric field of 300 MV/m. Gradually, the D–E loops are turned from a

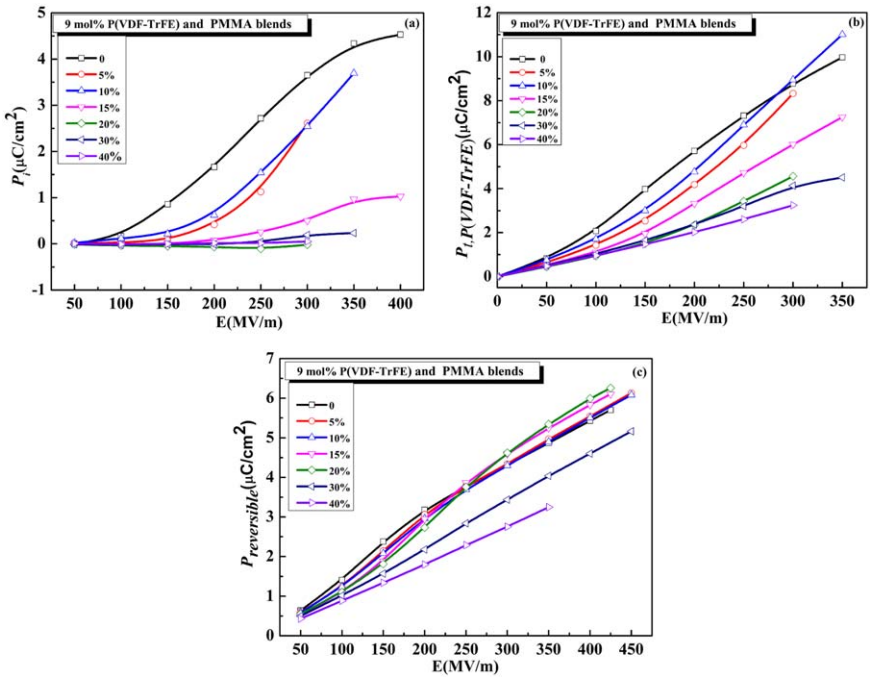

Figure 5. (a) Irreversible polarization of P(VDF-*co*-TrFE)/PMMA blends as a function of electric field calculated from eq. (3). (b) Contribution of P(VDF-*co*-TrFE)($P_{t,P(VDF\text{-}co\text{-}TrFE)}$) to P_{max} of P(VDF-*co*-TrFE)/PMMA blends as a function of electric field, which is calculated from eq. (4). (c) Reversible polarization of P(VDF-*co*-TrFE)/PMMA blends ($P_{reversible}$) as a function of electric field calculated by eq. (3). [Color figure can be viewed in the online issue, which is available at wileyonlinelibrary.com.]

rectangular shape into parallelogram-like shape and into linear-shape eventually when the PMMA content is over 30 wt %. The maximum polarization under AC electric field ($P_{max,AC}$) of the blend films is declining gradually as more PMMA is introduced into the system in general, which is mainly due to the lowered crystalline properties and the restricted flipping of ferroelectric phase induced by the addition of more PMMA with relative low polarity and high modulus. This result confirms the conclusion of dielectric response as discussed above. A step-like reduction of both P_{max} and remnant polarization (P_r) is observed when the PMMA content is 15 wt % and above this value the D–E loops show no more visible change. Besides, coercive field (E_c), the lowest electric field required to pole the ferroelectric phase, is vanishing in D–E loops of the blends as more PMMA is introduced, which suggests the much easier polarization of smaller ferroelectric domains as well as the polarization in crystal region are reduced although the blend are exposed under the high electric field.

Figure 4(b) compared the DC and AC loop of neat P(VDF-*co*-TrFE) under the same electric field at 375 MV/m. AC loops of blend films are not shown in this work. Clearly, the maximum polarization measured in AC and DC loop ($P_{max,AC}$ and $P_{max,DC}$) differs greatly from each other. The reason could be vividly illustrated by showing the domain orientation performance under external electric field in Figure 4(c,d). For a fresh sample, the dipoles are randomly aligned in the samples and the polarization in electric field direction is zero before the electric field applied as shown in status 1 in Figure 4(c). As external electric field increases, the dipoles start to align along the electric field direction and reach the maximum ($P_{max,\ DC}$) at the highest E [status 2 in Figure 4(c)]. As E decreases to zero, only a small portion of the dipoles aligned could be reversed ($P_{reversible}$) and most of them is maintained aligning to the direction of E [status 3 in Figure 4(c)]. After a short while, some of the remained polarization is relaxed (P_{relax}) and most of the polarization is left and stable for years [status 3′ in Figure 4(c)], which is well known as irreversible polarization (P_i) and where the excellent ferroelectric and piezoelectric properties of PVDF based ferroelectrics come from. In the next charging–discharging circle, the relatively small maximum polarization would be measured from status 5′ instead of status 1 to status 4. Meanwhile, the machine would automatically treat the polarization ending status of the last circle as the starting point (zero polarization) of next charging-discharging circle. Therefore, the P_i appeared in the first circle would not be observed in the next ones. The measurement both in AC and DC field in this work has a preloop process on the sample to test the stability of the sample before outputting data. That means all the D–E loops presented actually is from the second circle. The polarization process following the electric field applied could be seen more clearly in Figure 4(b), in which the curves with different color represent different polarization process, which has been more systematically illuminated as shown in Ref. 50. Apparently, comparing the D–E loops measured in AC and DC field becomes the only way to calculate the irreversible polarization (P_i) brought by big crystal domains.

From the above discussion, it can be drawn that $P_{max\ AC}$ of the samples driven by high AC electric field is composed of P_r and reversible polarization ($P_{reversible}$) two parts, where P_r is

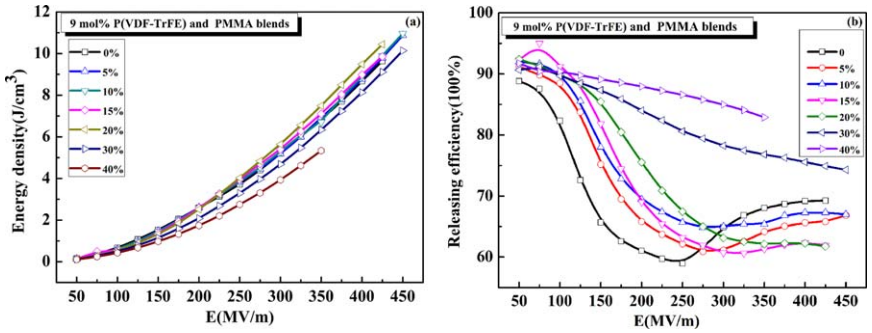

Figure 6. (a) Discharged energy density of P(VDF-*co*-TrFE)/PMMA blends. (b) Energy releasing efficiency of P (VDF-*co*-TrFE)/PMMA blends under different electric field. [Color figure can be viewed in the online issue, which is available at wileyonlinelibrary.com.]

contributed by both P_i of high polar crystal domains and the relaxed polarization (P_{relax}) induced by the polarization relaxation of amorphous phase and crystal domains. However, only $P_{reversible}$ and P_{relax} two parts are responsible for the $P_{max,DC}$, which means P_i is corresponding to the difference of P_{max} measured under AC and DC field. Namely,

$$P_{max,AC} = P_{reversible} + P_r = P_{reversible} + P_i + P_{relax} \quad (1)$$

$$P_{max,DC} = P_{reversible} + P_{relax} \quad (2)$$

$$P_i = P_{max,AC} - P_{max,DC} \quad (3)$$

P_i could be utilized to distinguish the relaxor ferroelectrics ($P_i = 0$) from the normal ferroelectrics ($P_i \neq 0$). Previous study has reported that P_i of P(VDF-*co*-TrFE) could be minimized to zero via introducing defects into the materials physically or chemically, where the typical ferroelectrics were turned into relaxed ferroelectrics. As shown in Figure 5(a), PMMA addition could also reduce P_i significantly as a function of applied electric field. When PMMA content is over 20 wt %, the P_i at 300 MV/m is decreased to about zero. That means P_i related to the crystal domains in large scale is effectively restricted thanks to both the dilution and impeding effect of PMMA on the crystalline properties of P(VDF-*co*-TrFE).

The confining effect of PMMA on the ferroelectric phase relaxation of P(VDF-*co*-TrFE) could be further illustrated by plotting $P_{max\ AC}$ of the blends contributed by P(VDF-*co*-TrFE) as a function of electric field since the polarization of blends could be regarded as the polarization sum of P(VDF-*co*-TrFE) and PMMA as follows:

$$P_{blends} = W_{PMMA} \times P_{PMMA} + W_{P(VDF-TrFE)} \times P_{t,P(VDF-TrFE)} \quad (4)$$

where W_{PMMA} and $W_{P(VDF-TrFE)}$ represent the weight percentage of PMMA and P(VDF-*co*-TrFE) in the blends, and W_{PMMA} and $P_{t,P(VDF\text{-}co\text{-}TrFE)}$ stand for the polarization contribution of PMMA and P(VDF-*co*-TrFE), respectively. The polarization of neat P(VDF-*co*-TrFE) under the electric field below 100 MV/m is nearly in linear against the increasing electric field mostly attributed to the polarization of amorphous phase and slight swing of crystal domains. When the applied electric field is over 100 MV/m, a sharp increment is observed at 100–300 MV/m field with a larger slope, which is mainly attributed to the flipping of ferroelectric phase driven by the applied electric field. PMMA addition leads to not only the higher driven electric field of ferroelectric phase flipping but also the lowered $P_{t,P(VDF\text{-}co\text{-}TrFE)}$ calculated from eq. (4) as shown in Figure 5(b). When PMMA is over 30 wt %, the linear increment of $P_{t,P(VDF\text{-}co\text{-}TrFE)}$ as a function of electric field up to 350 MV/m strongly indicates the flipping of ferroelectric phase in these samples is well depressed. That could be attributed to the effects of PMMA addition onto the crystalline properties of P(VDF-*co*-TrFE) including the reduced overall crystallinity thus the polarization of crystal phase and the improved modulus of amorphous phase, which may accelerate the disorientation of ferroelectric phase.

It is well addressed that only $P_{reversible}$ could follow the switching speed of the applied electric field, which is also responsible for the recoverable part of the stored electric energy greatly concerned for high-pulse capacitor applications. However, $P_{reversible}$ in ferroelectric P(VDF-*co*-TrFE) copolymer is rather low and is mainly attributed to the electronic and atomic polarization of P(VDF-*co*-TrFE) together with a few reversible polarization of small crystal domains. Although the P_{max} is significantly decreased due to the PMMA addition, $P_{reversible}$, calculated by either subtracting P_r from $P_{max,AC}$ as indicated in eq. (1) or subtracting P_{relax} from $P_{max,DC}$ as indicated in eq. (2), shows little reduction when PMMA content is no more than 20 wt %. When PMMA content is over 30 wt %, $P_{reversible}$ starts to reduce as shown in Figure 5(c). That might be attributed to the continuously lowered polarization contribution of PMMA than P(VDF-*co*-TrFE) and the restricted switching of small P(VDF-*co*-TrFE) crystal domains along the electric field. Meanwhile, the addition of rigid PMMA also leads to the enhanced discharging speed of the reversible polarization characterized with a reduced curvature of the discharging curves in D–E loops.

Energy Density and Loss of P(VDF-*co*-TrFE)/PMMA Blends

The energy storage and loss properties of dielectric materials are greatly concerned for high-pulse capacitor applications. When the electric field is applied on the dielectric materials, the dipoles in the crystal domains would switch to align with the external electric field direction. The switched dipoles would induce the generation of free charge on the surface of the dielectric field to form an internal electric field against the external electric field. Once the external electric field is removed, these free charges are supposed to release simultaneously along the elimination of the internal electric field referring to the disorientation of switched dipoles. Therefore, both the

discharge energy density and the discharging efficiency are dominated by the disorientation speed of switched dipoles. Figure 6(a) presents the discharged energy density of the blend films with varied PMMA content, which is calculated from the integral area under depolarization curve vs. electric displacement. Clearly, the discharged energy density of P(VDF-*co*-TrFE)/PMMA blends under the consistent electric field is well maintained when PMMA is added up to 30 wt %. When PMMA content is below 20 wt %, the discharged energy density of P(VDF-*co*-TrFE)/PMMA blends is even slightly higher than neat P(VDF-*co*-TrFE) owing to the restricted ferroelectric phase relaxation of P(VDF-*co*-TrFE), while more than 30 wt % PMMA addition leads to a continuous lowered energy density under the consistent electric field for the dilution effect of PMMA with low dielectric constant.

The released energy percentage, defined as $100 \times (U_{released}/U_{stored})\%$, is shown in Figure 6(b). The releasing efficiency of the charged energy in P(VDF-*co*-TrFE) is quickly reduced as electric field increases from 75 to 250 MV/m, and then increases gradually to a constant value when the electric field is over 300 MV/m. The peak formed at 100–300 MV/m field is attributed to the relaxation of ferroelectric phase along the electric field. As PMMA content increases, the switching of the crystal domains requires enhanced driven electric field for the confined flipping of ferroelectric phase together with the depressed crystalline properties of P(VDF-*co*-TrFE). When PMMA content is over 30 wt %, the lowered discharging efficiency induced by F–P transition is vanishing and the curve is turned into a linear shape, which means the switching of P(VDF-*co*-TrFE) crystal domains is completely vanished.

CONCLUSIONS

In general, the addition of rigid PMMA shows great influence onto the crystalline, dielectric, and electric energy storage properties of P(VDF-*co*-TrFE) containing 9 mol % TrFE for its dilution, impeding, and confining effect on the crystallization and ferroelectric phase relaxation of P(VDF-*co*-TrFE). PMMA addition may help the crystal phase transition from ferroelectric to ferroelectric relaxation phase of P(VDF-*co*-TrFE) at high electric field. The crystallinity, crystal size, the dielectric constant, and loss of P(VDF-*co*-TrFE) are reduced by the dilution and impediment effect of PMMA. Both the dilution and confinement effect of PMMA introduced onto the switch of polar P(VDF-*co*-TrFE) crystal domains results into the depressed polarization of blends under high electric field are characterized with dropped P_{max} and P_i. The blends are turned from normal ferroelectrics to relaxed ferroelectrics and even linear shaped dielectrics, thus the unreleased energy is significantly reduced while the discharge energy density is well maintained. Both the reduced crystalline properties and the depressed switching of crystal domains under high electric field are responsible for the improved electrical performance of the blends. The blend with 30 wt % PMMA exhibits the most desirable dielectric performance for high-pulse capacitor utilization, with an energy storage density of about 10 J/cm^{-3} but an unreleased energy loss percentage less than 25%.

ACKNOWLEDGMENTS

This work was financially supported by National Nature Science Foundation of China-NSAF (Grant No. 51103115, 50903065, and 12JK0441), Fundamental Research Funds for the Central Universities, Beijing National Laboratory for Molecular Sciences (BNLMS), Program for New Century Excellent Talents in University and International Science & Technology Cooperation Program of China (Grant No.2010DFR50480).

REFERENCES

1. Kawai, H. *Jpn. J. Appl. Phys.* **1969**, *8*, 975.
2. Higashihata, Y.; Sako, J.; Yagi, T. *Ferroelectrics* **1981**, *32*, 85.
3. Tajitsu, Y.; Chiba, A.; Furukawa, T.; Date, M.; Fukada, E. *Appl. Phys. Lett.* **1980**, *36*, 286.
4. Sarjeant, W. J. *IEEE Trans. Electr. Insul.* **1990**, *25*, 861.
5. Sarjeant, W. J.; Zirnheld, J.; MacDougall, F. W. *IEEE Trans. Plasm. Sci.* **1998**, *26*, 1368.
6. Sarjeant, W. J.; Zirnheld, J.; Price, R. A. *Proc. IEEE* **2001**, *26*, 846.
7. Lam, K. H.; Chan, H. L. W. *J. Appl. Phys.* **2004**, *96*, 5898.
8. MacDougall, F. W.; Yang, X. H.; Ennis, J. B.; et al. IEEE 12th Symposium on Electromagnetic Launch Technology, Snowbird, UT, USA. **2004**, 294–232.
9. Zhang, Q. M.; Bharti, V.; Zhao, X. *Science* **1998**, *280*, 2101.
10. Xu, H. S.; Cheng, Z. Y.; Olson, D.; Mai, T.; Zhang, Q. M.; Kavarnos, G. *Appl. Phys. Lett.* **2001**, *78*, 2360.
11. Chung, T. C. M.; Petchsuk, A. *Macromolecules* **2002**, *35*, 7678.
12. Wang, Z. M.; Zhang, Z. C.; Chung, T. C. M. *Macromolecules* **2006**, *39*, 4268.
13. Lu, Y. Y.; Claude, J.; Neese, B.; Zhang, Q. M.; Wang, Q. *J. Am. Chem. Soc.* **2006**, *128*, 8120.
14. Lu, Y. Y.; Claude, J.; Zhang, Q. M.; Wang, Q. *Macromolecules* **2006**, *39*, 6962.
15. Chu, B. J.; Zhou, X.; Ren, K. L.; Neese, B.; Lin, M. R.; Wang, Q.; Bauer, F.; Zhang, Q. M. *Science* **2006**, *313*, 334.
16. Guan, F. X.; Pan, J. L.; Wang, J.; Wang, Q.; Zhu, L. *Macromolecules* **2010**, *43*, 384.
17. Zhou, X.; Chu, B. J.; Neese, B.; Lin, M. R.; Zhang, Q. M. *IEEE Trans. Dielec. Electr. Insul.* **2007**, *14*,1133.
18. Chen, X. Z.; Li, Z. W.; Cheng, Z. X.; Zhang, J. Z.; Shen, Q. D.; Ge, H. X.; Li, H. T. *Macromol. Rapid Commun.* **2011**, *32*, 94.
19. Xia, W. M.; Xu, Z.; Wen, F.; Li, W. J.; Zhang, Z. C. *Appl. Phys. Lett.* **2010**, *97*, 222905.
20. Guan, F. X.; Wang, J.; Pan, J. L.; Wang, Q.; Zhu, L. *Macromolecules* **2010**, *43*, 6739.
21. Guan, F. X.; Wang, J.; Yang, L. Y.; Tseng, J. K.; Han, K.; Wang, Q.; Zhu, L. *Macromolecules* **2011**, *44*, 2190.
22. Guan, F. X.; Yang, L. Y.; Wang, J.; Guan, B.; Han, K.; Wang, Q.; Zhu, L. *Adv. Funct. Mater.* **2011**, *21*, 3176.

23. Saito, K.; Miyata, S.; Wang, T. T.; Jo, Y. S.; Chujo, R. *Macromolecules* **1986**, *19*, 2452.
24. Tsutsumi, N.; Ono, T.; Kiyotsukuri, T. *Macromolecules* **1993**, *26*, 5447.
25. Burgel, A.; Kleeman, W.; Biebricher, M. *Franke. Appl. Phys. A* **1995**, *60*, 475.
26. Faria, L. Q.; Moreira, R. L. *Polymer* **1999**, *40*, 4465.
27. Kim, K. J.; Kim, G. B.; Han, S. H. *J. Appl. Polym. Sci.* **1993**, *49*, 7.
28. Faria, L. Q.; Moreira, R. L. *J. Polym. Sci. Part B: Polym. Phys.* **1999**, *38*, 34.
29. Kim, K. J.; Kim, G. B. *J. Appl. Polym. Sci.* **1993**, *47*, 1781.
30. Faria, L. Q.; Moreira, R. L. *J. Polym. Sci. Part B: Polym. Phys.* **1999**, *37*, 2996.
31. Meng, Q. J.; Li, W. J.; Zheng, Y. S.; Zhang, Z. C. *J. Appl. Polym. Sci.* **2010**, *116*, 2674.
32. Tan, S. B.; Liu, E. Q.; Zhang, Q. P.; Zhang, Z. C. *Chem. Commun.* **2011**, *47*, 4544.
33. Koga, K.; Nakano, N.; Hattori, T.; Ohigashi, H. *J. Appl. Phys.* **1990**, *67*, 965.
34. Zhang, G. Z.; Kitamura, T.; Yoshida, H.; Kawai, T. *Netsu. Sokutei.* **2002**, *29*, 192.
35. Cheng, Z. Y.; Bharti, V.; Xu, T. B.; Wang, S. X.; Zhang, Q. M.; Ramotowski, T.; Tito, F.; Ting, R. *J. Appl. Phys.* **1999**, *86*, 2208.
36. Imamura, R.; Silva, A. B.; Gregorio, Jr, R. *J. Appl. Polym. Sci.* **2008**, *110*, 3242.
37. Li, W. J.; Meng, Q. J.; Zheng, Y. S.; Zhang, Z. C. *Appl. Phys. Lett.* **2010**, *96*, 192905.
38. Yagi, T.; Tatemoto, M.; Sako, J. *Polym. J.* **1980**, *12*, 209.
39. Sajkiewicz, P. *Eur. Polym. J.* **1999**, *35*, 1581.
40. Chen, S. T.; Yao, K.; Tay, F. E. H.; Chew, L. L. S. *J. Appl. Polym. Sci.* **2010**, *116*, 3331.
41. Zhang, Q. P.; Xia, W. M.; Zhu, Z. G.; Zhang, Z. C. *J. Appl. Polym. Sci.* **2013**, *127*, 3002.
42. Martins, P.; Lopesa, A. C.; Lanceros-Mendeza, S. *Prog. Polym. Sci.* http://dx.doi.org/10.1016/j.progpolymsci.2013.07.006.
43. Li, M. Y.; Stingelin, N.; Michels, J. J.; Spijkman, M. J.; Asadi, K.; Feldman, K.; Blom, P. W. M.; De Leeuw, D. M. *Macromolecules* **2012**, *45*, 7477.
44. Ranjan, V.; Nardelli, M. B.; Bernhole, J. E. *Phys. Rev. Lett.* **2012**, *108*, 087802–1.
45. Sencadas, V.; Lanceros-Méndez, S.; Sabater i Serra, R.; Andrio Balado, A. J.; Gómez Ribelles. J. L. *Eur. Phys. J. E* **2012**, *85*, 41.
46. Furukawa, T.; Wang, T. In The Applications of Ferroelectric Polymers; Wang, T., Herbert, J. M., Glass, A. M., Eds.; Chapman & Hall: New York, **1988**; Vol. *5*, p 66.
47. Hahn, B.; Wendorff, J.; Yoon, D. Y. *Macromolecules* **1985**, *18*, 718.
48. Sy, J. W.; Mijovic, J. *Macromolecules* **2000**, *33*, 933.
49. Chandra, A.; Meyer, W. H. *J. Appl. Polym. Sci.* **2013**, *127*, 2857.
50. Zhang, Z. C.; Chung, T. C. M. Energy storage of poly(vinylidene fluoride) (PVDF) based fluoropolymer. In: Advances in Energy Research. Volume 2; Acosta, M. J., Ed.; Nova Science Publishers Inc.: New York, **2011**; pp. 129–164.